Mixed-mode fracture and load misalignment on the assessment of FRP-concrete bond connections

P. Neto[a,*], J. Alfaiate[b], D. Dias-da-Costa[c,d], J. Vinagre[a]

[a]ICIST and Escola Superior de Tecnologia do Barreiro, Setubal Polytechnic Institute, Rua Américo da Silva Marinho, 2839-001 Lavradio, Barreiro, Portugal

E-mail: pedro.neto@estbarreiro.ips.pt

E-mail: joao.vinagre@estbarreiro.ips.pt

[b]ICIST, Department of Civil Engineering and Architecture, Instituto Superior Técnico, University of Lisbon, Av. Rovisco Pais 1, 1049-001 Lisboa, Portugal

E-mail: jorge.alfaiate@tecnico.ulisboa.pt

[c]School of Civil Engineering, The University of Sydney, NSW2006, Australia

[d]ISISE, Department of Civil Engineering, University of Coimbra, Rua Luís Reis Santos, 3030–788 Coimbra, Portugal

E-mail: daniel.diasdacosta@sydney.edu.au

[*]Corresponding author: Tels.: +351 964 444 103; +351 212 064 660; Fax: +351 212 075 002

Escola Superior de Tecnologia do Barreiro, Setubal Polytechnic Institute, Rua Américo da Silva Marinho, 2839-001 Lavradio, Barreiro, Portugal

E-mail: pedro.neto@estbarreiro.ips.pt

Abstract

Considerable dispersion is usually found in experimental data concerning the material properties of FRP-concrete bond connections. In pure shear models, the direction of FRP loading is assumed to be parallel to the axis of the concrete specimen. However, in practice, it is very difficult to prevent load misalignment. This fact can have important consequences on the derivation of material properties from experimental data. This is why a parametric study is herein undertaken to thoroughly identify the role of the load misalignment in the behaviour of the connection. It is concluded that the load capacity of the connection significantly decreases in the case of a

Post-print: Neto, P., Alfaiate, J., Dias-da-Costa, D., Vinagre, J., Mixed-mode fracture and load misalignment on the assessment of FRP-concrete bond connections, *Composite Structures*, Elsevier, 135:49–60, 2016 (doi: 10.1016/j.compstruct.2015.08.139).

misaligned load pointing outwards the reinforced surface. It is also found that this effect is less relevant for thick laminates when compared to thin FRP sheets.

Keywords: FRP-concrete bond behaviour; Fibre Reinforced Polymers (FRP); Mixed-mode fracture; Load misalignment; Numerical modelling.

1. Introduction

The use of fibre reinforced polymers (FRP) for external strengthening of concrete structures, particularly in the form of laminates and sheets, has become quite common. This is related to both the competitive mechanical properties of the composite material, e.g. in the form of high strength-to-weight ratio, and the straightforward in-situ installation. However, the use of this technique requires that local failure modes are duly accounted for. In the last few years, the scientific community has been quite active and important experimental and analytical contributions were given towards a better understanding and prediction of the bond behaviour between concrete and FRP, as mentioned below.

There are still several issues that require a clarification in the quantification of the bond between concrete and strengthening material. Various authors have adopted pure shear test models to derive constitutive relationships for the concrete-to-FRP interface, e.g. [1-6]. In these models it is assumed that the FRP loading: i) is applied parallel to the axis of the concrete specimen; and ii) is perfectly aligned with the symmetry axis of the strengthened material. Unfortunately, as it will be shown, a variety of models exist and a considerable dispersion of the parameters characterising the bond behaviour have been reported. Furthermore, the stress distribution on pure shear test models does not precisely match the one obtained in bending reinforcement; in the latter case, besides tangential stress, several authors argued on the importance of the normal stresses developing in the connection [3, 4, 7-9]. In particular, mixed-mode debonding in a peel test configuration was modelled by De Lorenzis and Zavarise in [10].

Post-print: Neto, P., Alfaiate, J., Dias-da-Costa, D., Vinagre, J., Mixed-mode fracture and load misalignment on the assessment of FRP-concrete bond connections, *Composite Structures*, Elsevier, 135:49–60, 2016 (doi: 10.1016/j.compstruct.2015.08.139).

The stress concentration occurring at the extremity of the FRP can lead to premature collapse of the strengthened concrete beam. This type of local failure generally occurs along a thin concrete layer attached to the epoxy-fibre layers, the latter remaining intact. The importance of this phenomenon is related to the energy dissipated per unit of cracked surface, which involves a combination of both mode-I and mode-II fracture, designated by mixed mode fracture. Several experimental and numerical tests have been carried out to study this behaviour. However, the definition of these material parameters is still not well established and contradictory results are found. For instance, Bazant and Pfeiffer [11] and Ozbolt, Reinhardt [12] proposed mode-II fracture energy values *circa* 25 times greater than the fracture energy, whereas Täljsten [4] proposed a ratio of approximately 10 after experimental tests submitting the specimen to both compression and shear stresses.

2. Research significance

The above reported issues have often been neglected in the literature in spite of their importance for the accurate prediction of the bond behaviour of FRP-concrete connections. This manuscript aims at contributing to the present state-of-the-art by undertaking a comprehensive numerical study to:

- quantify the relevance of the load misalignment in pure shear test models and corresponding errors in the interpretation of existing experimental data;
- evaluate the importance of mixed-mode facture and mode-II fracture energies in the analysis of existing experimental data;
- identify the role of all above parameters in the maximum load and effective bond length attained by a connection.

As it will be shown in the following sections, these aspects are critical for the development of accurate models capable of predicting the bond behaviour of FRP-concrete connections and for the interpretation of existing experimental data.

Post-print: Neto, P., Alfaiate, J., Dias-da-Costa, D., Vinagre, J., Mixed-mode fracture and load misalignment on the assessment of FRP-concrete bond connections, *Composite Structures*, Elsevier, 135:49–60, 2016 (doi: 10.1016/j.compstruct.2015.08.139).

The manuscript is organised as follows. A review is presented in Section 3 concerning existing models, constitutive laws and corresponding material properties relevant to the behaviour of a FRP-concrete connection. Next, in Section 4, the numerical model is defined. In Section 5, a parametric study is undertaken to assess the role of the different parameters in the maximum load and effective bond length of a connection. Finally, the most important conclusions are summarised in Section 6.

3. Literature review

3.1. Bond models and constitutive law

Several authors have reported that debonding occurs mainly due to the shear failure of concrete. Different setups have been proposed: the single shear test shown in Fig. 1 [13-15], the double shear test [16] and the flexural test [13, 16, 17]. Unfortunately, there is still not a single pre-defined test and the conclusions drawn by different authors strongly depend on the selected setup [18].

Currently, there are numerous models describing the bond behaviour, such as empirical or semi-empirical formulations, closed-form analytical and numerical models. Fracture Mechanics is also adopted by several authors, either using Linear-Elastic Fracture Mechanics, e.g. [10, 15, 19], or Nonlinear Fracture Mechanics, e.g. [4, 20]. The debonding mechanism between composite and substrate can be modelled using interface elements equipped with a local bond-slip law [14, 16, 17, 21-26]; conversely, in some cases, perfect bond is also assumed with good results [3, 27-30]. Other class of numerical strategies avoid the use of interface elements, by employing a smeared crack model to predict debonding using an appropriate constitutive law for concrete [13, 31].

A linear elastic bond-slip without softening was initially used for modelling steel plates externally bonded to concrete [32-35]. Later on, authors like Yuan, Wu [20], Lee, Boothby [36] and Täljsten [4] have applied this formulation to FRP bonded to concrete. However, a more accurate prediction of the bond behaviour requires the modelling of the concrete softening behaviour. In this case,

Post-print: Neto, P., Alfaiate, J., Dias-da-Costa, D., Vinagre, J., Mixed-mode fracture and load misalignment on the assessment of FRP-concrete bond connections, *Composite Structures*, Elsevier, 135:49–60, 2016 (doi: 10.1016/j.compstruct.2015.08.139).

there are different available approximations for the softening law: linear [20, 24, 37, 38]; bilinear (non-null slope) [39, 40]; or exponential [20, 23], among others [15-17]. Several authors, namely Ferracuti, Savoia [21], Nakaba, Kanakubo [41] and Savoia, Ferracuti [14], have applied a power fractional law based on the work of Popovics [42] in order to describe the interfacial behaviour. A comprehensive review on bond-slip models can be found in [22] and [16].

The bilinear and exponential bond-slip laws were initially adopted for mode-I fracture by Petersson [43] in the simulation of concrete bending beams. These relationships are known to represent correctly the concrete behaviour under softening. Since in most cases the debonding process occurs within the concrete, these laws were successfully extended, with good results, to mode-II fracture in [40, 44]. This latter approach will be further discussed in the following sections.

3.2. Material parameters

The definition of a bond-slip law requires several parameters, namely: *i*) interfacial stiffness, k_s; *ii*) cohesion, *c*; and *iii*) mode-II fracture energy, G_F^{II} (see Fig.2). The most relevant work carried out to quantify all these parameters is summarised in the following sections.

3.2.1. Interfacial stiffness

Lu, Jiang [31] developed a numerical model without explicit consideration of the adhesive layer by assuming that both the elastic deformation of the adhesive layer and interfacial slip on the failure process are insignificant. Also based on the adhesive properties, Wang [17] obtained an elastic shear stiffness value of 153 MPa/mm for a resin adhesive layer with 2.5 mm average thickness and 0.992 GPa Young's modulus.

According to De Lorenzis, Miller [45], and particularly in the case of *in situ* cured systems, the shear stiffness should take into account the contribution of the set of applied resins. They propose a value of k_s = 383 MPa/mm.

Post-print: Neto, P., Alfaiate, J., Dias-da-Costa, D., Vinagre, J., Mixed-mode fracture and load misalignment on the assessment of FRP-concrete bond connections, *Composite Structures*, Elsevier, 135:49–60, 2016 (doi: 10.1016/j.compstruct.2015.08.139).

Bizindavyi and Neale [6] observed that the surface preparation of the concrete also plays an important role on the shear stiffness. Having this under consideration, Brosens [46] suggested values of 1501 MPa/mm, 1687 MPa/mm, 1873 MPa/mm for the shear stiffness, whereas Ferracuti, Savoia [21] proposed a value of 226.61 MPa/mm.

Ali-Ahmad, Subramaniam [47] used a different approach based on quasi-static monotonic tests on FRP composite bonded to concrete, estimating a shear stiffness of 104.8 MPa/mm.

It is quite clear that the values proposed by the authors vary significantly. As previously mentioned, this is due to different: *i*) experimental models; *ii*) material properties (substrate, composite and adhesive); and *iii*) preparation of the concrete surface.

3.2.2. Cohesion

In most situations, failure occurs with the detachment of a thin concrete layer neighbouring the interface. In this case, the concrete properties become much more relevant for the connection. Several authors, like Arduini and Nanni [48], Arduini, DiTommaso [49], Brosens [46], Chajes, Finch [5], Ebead and Neale [23], Holzenkämpfer [37] and Nakaba, Kanakubo [41], presented a relation between concrete properties and maximum tangential stress. Brosens [46], Ebead and Neale [23] and Holzenkämpfer [37] also considered the width of FRP and concrete. The first two aforementioned authors additionally took into account the surface preparation of the substrate. Later on, Pellegrino and Modena [16] proposed the following expression using experimental results in [50]:

$$\tau_{\max} = 3.1\left(n_f t_f E_f\right)^{0.32}, \tag{1}$$

where $n_f t_f$ is the total thickness and E_f the elastic modulus of the FRP.

The chart depicted in Fig. 3 contains a summary of the cohesion values proposed by several authors, shown as a function of the concrete compressive strength. From these results, it is possible to highlight a relative dispersion, with the smaller and highest values found, respectively,

Post-print: Neto, P., Alfaiate, J., Dias-da-Costa, D., Vinagre, J., Mixed-mode fracture and load misalignment on the assessment of FRP-concrete bond connections, *Composite Structures*, Elsevier, 135:49–60, 2016 (doi: 10.1016/j.compstruct.2015.08.139).

in Brosens [46] and Pellegrino and Modena [16]. In general, the adopted cohesion lies between 5 and 7 MPa for normal concrete.

3.2.3. Mode-II fracture energy

The mode-II fracture energy, G_F^{II}, is defined as the energy dissipated per unit area of shear interface under the absence of normal tractions. Täljsten [4] designed a set of experimental tests for measuring G_F^{II}, where a concrete specimen was simultaneously submitted to shear and compressive stresses. The authors proposed values in the range of 1210.7 ± 462.9 Nm/m^2, for a mean concrete tensile strength of 4.1 MPa.

Neubauer and Rostásy [38] proposed the following expression using the average value of the concrete tensile strength, f_{ctm}:

$$G_F^{II} = c_F^{II} f_{ctm}, \tag{2}$$

where c_F^{II} is an empirical constant dependent on the experimental results, for which the authors proposed the value of 0.204 mm.

A more comprehensive approach was followed by Brosens [46] and Holzenkämpfer [37] who took into account both FRP and concrete section widths, as well as the surface preparation, leading to the following relation:

$$G_F^{II} = k_b^2 k_c^2 c_F^{II} f_{ctm}, \tag{3}$$

where k_b is a width factor, k_c takes into account the surface preparation of the concrete surface and c_F^{II} is a parameter taking the value of 0.40 mm.

In Lu, Teng [51] simplified models are presented to evaluate G_F^{II}, which can be calculated as:

$$G_F^{II} = 0.308 \beta_w^2 \sqrt{f_t}, \tag{4}$$

where f_t is the concrete tensile strength and β_w is given by:

Post-print: Neto, P., Alfaiate, J., Dias-da-Costa, D., Vinagre, J., Mixed-mode fracture and load misalignment on the assessment of FRP-concrete bond connections, *Composite Structures*, Elsevier, 135:49–60, 2016 (doi: 10.1016/j.compstruct.2015.08.139).

$$\beta_w = \sqrt{\left(2.25 - b_f / b_c\right) / \left(1.25 + b_f / b_c\right)}. \quad (5)$$

The previous expression includes the effect of the relation between adherent and substrate widths, respectively b_f and b_c. However, the concrete surface preparation is not considered.

The values of mode-II fracture energy estimated from the studies of Ali-Ahmad, Subramaniam [24] and Pellegrino and Modena [16], based on previous works [47, 50], are shown in Fig. 4. According to Pellegrino and Modena [16] G_F^{II} can be estimated by:

$$G_F^{II} = \frac{\tau_{max} s_{peak}}{1.575} + \frac{\tau_{max}}{\left(s_{peak}^{\gamma} - s_{ult}^{\gamma}\right)(\gamma + 1)}\left(s_{ult}^{\gamma} s_{peak}^{\gamma} - s_{peak}^{\gamma+1}\right), \quad (6)$$

where s_{peak} is the slip at maximum bond stress and s_{ult} is the slip when bond stress decays to zero, given by:

$$s_{peak} = 0.075\left(n_f t_f E_f\right)^{0.2}, \quad (7)$$

$$s_{ult} = 10.5\left(n_f t_f E_f\right)^{0.6} \quad (8)$$

and γ is given by:

$$\gamma = \frac{1.3162}{\left(n_f t_f E_f\right)^{0.187}}. \quad (9)$$

The value of τ_{max} is obtained by applying Eq. (1).

Savoia, Ferracuti [14] applied inverse analysis for the calibration of the bond law and to estimate the interfacial fracture energy. Several authors, such as Ferracuti, Savoia [21], Neto, Alfaiate [40] and Wang [17], estimated the mode-II fracture energy from the value of the ultimate load, N_u. The most common expression is given in Eq. (10), valid if the axial stiffness ratio between concrete and FRP is significantly above the unity:

$$N_u = b_f \sqrt{2 G_F^{II} E_f t_f}, \quad (10)$$

where b_f and t_f are the width and the thickness of the FRP, respectively.

Post-print: Neto, P., Alfaiate, J., Dias-da-Costa, D., Vinagre, J., Mixed-mode fracture and load misalignment on the assessment of FRP-concrete bond connections, *Composite Structures*, Elsevier, 135:49–60, 2016 (doi: 10.1016/j.compstruct.2015.08.139).

The relevance of the mode-II fracture energy on the bond strength is shown in the last equation, although it does not allow relating G_F^{II} directly with the properties of the materials involved.

In Fig. 4 a brief overview of G_F^{II} values presented by several authors is shown, as a function of the concrete compressive strength. It is assumed that G_F^{II} is a material property and other material properties eventually affecting its value are neglected. The represented results exhibit a dispersion higher than the one found for the cohesion (see Fig. 3). For concrete commonly used in buildings, the ratio between maximum and minimum values of G_F^{II} can reach nearly four. This is again related to the diversity of adopted procedures, models and assumptions used in the quantification of the bond behaviour.

4. Numerical model

4.1. Pure shear model

The numerical shear model considered in this work is based on the experimental tests performed at Instituto Superior Técnico Travassos [52]. These tests consisted of concrete specimens in which unidirectional carbon fibres were glued by means of resin epoxy. The specimen, a single shear test under tension-compression (Fig. 1), was subjected to a tensile load along the direction of the fibres, as shown in Fig. 5. The concrete specimens tested exhibited a rectangular cross-section of 200 mm by 200 mm. and were 400 mm long. In this study, taking into account the adopted thickness, maximum lengths of 500 mm and 1000 mm are considered, in order to guarantee that the specimen length has no influence on the analysis. The strengthening material was 80 mm wide and 0.111 mm thick, and was applied on the larger face of the specimen. The nominal values for Young's modulus and for the ultimate tensile strain of the CFRP were 240 GPa and 15.5‰, respectively. Mean values of 36.4 MPa, 2.8 MPa and 31.6 GPa, for the compressive strength, tensile strength and Young's modulus of concrete, respectively, were considered.

Post-print: Neto, P., Alfaiate, J., Dias-da-Costa, D., Vinagre, J., Mixed-mode fracture and load misalignment on the assessment of FRP-concrete bond connections, *Composite Structures*, Elsevier, 135:49–60, 2016 (doi: 10.1016/j.compstruct.2015.08.139).

4.2. Material models

Concrete is herein considered as a rigid substrate, whereas a linear elastic behaviour is assumed for the FRP. The bond between concrete, resin and CFRP is modelled using interface elements with zero initial thickness in the scope of a discrete crack approach. A multi-surface plasticity model is adopted from [53-55], in which two limit surfaces are considered: a tension cut-off for mode-I fracture given by the concrete tensile strength and a Coulomb friction envelope for mode-II and mixed-mode fracture, as shown in Fig. 6. In this figure, the horizontal axis represents the stress component normal to the interface, whereas the vertical axis represents the tangential stress component parallel to the interface.

The Coulomb friction envelope is initially characterised by the cohesion coefficient and by the internal friction angle ϕ, where both yield functions follow an exponential softening flow rule (Fig. 7). The yield function associated with the normal stress is given by:

$$f_n = \sigma_n - f_t \exp\left(-\frac{f_t}{G_F} w\right), \tag{11}$$

where σ_n is the stress vector normal component measured at the interface and w is the opening in the direction normal to the interface. An associated flow rule is considered. The shear yield function reads:

$$f_s = |\tau| + \sigma_s \tan\phi - c \exp\left(-\frac{c}{G_F^{II}} s\right), \tag{12}$$

where τ is the tangential stress vector component measured at the interface and s is the relative displacement in the direction tangential to the interface, i.e. the slip. In this case, a non-associated flow rule is adopted with a plastic potential, g_s, given by:

$$g_s = |\tau| + \sigma_n \tan\psi - c, \tag{13}$$

where ψ is the dilatancy angle.

Post-print: Neto, P., Alfaiate, J., Dias-da-Costa, D., Vinagre, J., Mixed-mode fracture and load misalignment on the assessment of FRP-concrete bond connections, *Composite Structures*, Elsevier, 135:49–60, 2016 (doi: 10.1016/j.compstruct.2015.08.139).

An isotropic softening criterion is adopted, meaning that both yield surfaces shrink the same relative amount in the stress space and keep the origin.

The material parameters characterising the interface behaviour are the following: *i*) elastic shear and peeling stiffness, k_s and k_n, respectively; ii) cohesion c; iii) tensile strength f_t; and iv) fracture energies in mode-I and mode-II, G_F and G_F^{II}, respectively. These fracture energies are represented in Fig. 7 as the areas under the curves σ_n-w and τ-s, respectively.

4.3. Numerical solution

Two different finite element meshes are selected for undertaking the numerical simulations: one for pure mode-II fracture analysis and a second one for mixed-mode fracture analysis [40]. In pure mode-II fracture models (reference models), bilinear 4-node isoparametric elements are considered for the concrete, whereas truss elements are applied to model the strengthening material, as shown in Fig. 8 (a). In the models used for mixed-mode fracture analysis, bilinear 4-node isoparametric elements are used for both concrete and the strengthening material, as illustrated in Fig. 8 (b). In both cases, linear zero thickness interface elements are used to model the bond behaviour.

The specimen response is computed under displacement control, using an incremental and iterative procedure based on both the Newton-Raphson method and the arc-length algorithm.

4.4. Adopted parameters

As mentioned above, the constitutive relationship of the interface concrete-CFRP is defined by the following parameters: *i*) shear and peeling stiffness; *ii*) cohesion; *iii*) tensile strength; and *iv*) fracture energies, both in mode-I and mode-II fracture. Based on a study presented in [40, 56], the following values are adopted: k_s = 1500 MPa/mm and k_n = 4000 MPa/mm, respectively for the shear and peeling stiffness; c = 5 MPa for the cohesion and G_F = 0.1 N/mm for the fracture energy in mode-I fracture. According to the literature, the ratio between mode-I and mode-II

Post-print: Neto, P., Alfaiate, J., Dias-da-Costa, D., Vinagre, J., Mixed-mode fracture and load misalignment on the assessment of FRP-concrete bond connections, *Composite Structures*, Elsevier, 135:49–60, 2016 (doi: 10.1016/j.compstruct.2015.08.139).

fracture energies can vary between 10 and 25 [4, 11, 12, 57, 58]. An intermediate value is considered, leading to G_F^{II} = 1.5 N/mm.

Angle α is defined in Fig. 9 as the angle between applied force and longitudinal direction of the glued surface. Different values are taken to study the effect of the load misalignment, i.e.: α = ±0.5º, α = ±1.0º, α = ±1.5º and α = ±2.0º, where $\alpha > 0$º and $\alpha < 0$º represent the normal component of the applied load pointing, respectively, outwards and inwards with respect to the substrate. As a consequence, in addition to the tangential stresses, normal stresses are also expected to develop at the interface.

The CFRP thickness is variable, i.e.: t_f = 0.1 mm, t_f = 0.5 mm, t_f = 1.4 mm and t_f = 6.0 mm. In all cases, the adopted bond length, l_b, is higher than the effective bond length. The numerical findings are thoroughly presented and discussed in the following section.

5. Numerical findings

This section addresses the role of the CFRP thickness and load misalignment in the behaviour of the connection and derivation of constitutive parameters from experimental data.

5.1. CFRP thickness

The role of the CFRP thickness in the stress distribution is herein addressed. The obtained results are shown in Fig. 10 for an intermediate load level corresponding to 65% of the maximum load, N_{max}, achieved using the pure mode-II fracture model. The x-axis is defined in Fig. 9.

For thinner strengthening solutions, no significant differences are found in the developing bond stresses, as shown in Figs.10 (a) to (c). For the thickest strengthening solution, mixed-mode fracture becomes important (see Fig. 10(d)), although this solution is too thick for common practice. From Fig. 10 it can be observed that normal stresses develop in addition to the shear stress when the CFRP is modelled using four node finite elements. These normal stresses are

Post-print: Neto, P., Alfaiate, J., Dias-da-Costa, D., Vinagre, J., Mixed-mode fracture and load misalignment on the assessment of FRP-concrete bond connections, *Composite Structures*, Elsevier, 135:49–60, 2016 (doi: 10.1016/j.compstruct.2015.08.139).

compressive, located in a small area close to the applied load, and are caused by the lever arm developing at the CFRP thickness (see Fig. 11).

5.2. Load misalignment

In this Section, the influence of the deviation angle of the applied load with respect to the element axis is analysed in a pure shear model. The following situations are considered concerning the direction of the normal component of the applied load: pointing inwards the substrate and pointing outwards the substrate.

5.2.1. Normal component pointing inwards the substrate

The interfacial stress distribution along the bond length is obtained for a composite thickness of 0.1 mm and $\alpha = -1.0º$. In Fig. 12 the interfacial stresses concrete-CFRP are presented along the bond length at about 20% and 90% of the maximum load found in that model, which is approximately 22.5 kN.

For lower load levels, the shear stresses tend to become higher than the initial cohesion due to the presence of normal compressive stresses, in accordance to the yield surface shown in Fig. 6. These stresses occur only along a short length, in the vicinity of the applied load. Apart from the region where normal stresses co-exist, the shear stress distribution becomes similar to the one obtained in a pure shear model as shown in [40].

In Fig. 13 the interfacial stresses developing along the bond length are shown, in the case of a composite thickness of 0.5 mm and $\alpha = -1.0º$, at 20% and 90% of the maximum load registered in the model, i.e. circa 48 kN. In this case, the normal compressive stresses span over a longer length than the one observed with t_f = 0.1 mm. Outside this region, once again the shear stress distribution becomes similar to the one obtained in a pure shear model.

Post-print: Neto, P., Alfaiate, J., Dias-da-Costa, D., Vinagre, J., Mixed-mode fracture and load misalignment on the assessment of FRP-concrete bond connections, *Composite Structures*, Elsevier, 135:49–60, 2016 (doi: 10.1016/j.compstruct.2015.08.139).

5.2.2. Normal component pointing outwards the substrate

In this Section the effect of a positive misalignment angle, $\alpha > 0^{\circ}$, is analysed (see Fig. 9). In Fig. 14, the interfacial stresses along the bond length are represented for a CFRP thickness of 0.1 mm, when applied loads are close to 20% and 90% of the maximum load (approximately 9.5kN). Except for the region where normal stresses develop, the shear stress distribution becomes similar to the one obtained in the pure shear model [40]. Also in this case, normal/peeling stresses develop in the interface in a small length near the applied load.

In Fig. 15 the results obtained in the case of a CFRP with 0.5 mm thickness are shown, also for 20% and 90% of the maximum load, which is approximately 25 kN. The conclusions are similar to the ones found for the thinnest CFRP.

5.2.3. Comparative discussion

For t_f = 0.1 mm and $\alpha = +1.0^{\circ}$ the maximum load is *circa* 42% of the maximum load obtained for $\alpha = -1.0^{\circ}$. Since the experimental assessment of the mode-II fracture energy strongly depends on the ultimate load (see Eq. (10)), unreliable values can result for this parameter. This issue will be further discussed below.

Results obtained with $\alpha \neq 0^{\circ}$ and with $\alpha = 0^{\circ}$ are shown in Fig. 16 for a load level of 65% of the maximum load reached with $\alpha = -1.0^{\circ}$ and $\alpha = +1.0^{\circ}$, i.e., respectively 15 kN and 6 kN. Both maximum load and shear stress distributions are quite similar for $\alpha = -1.0^{\circ}$ and $\alpha = 0^{\circ}$, except in a short length near the location of the applied load, as shown in Fig. 16(a). Therefore, in this case, a satisfactory quantification of the material parameters can be achieved from experimental data, namely: k_s, c and G_F^{II}.

When $\alpha = +1.0^{\circ}$ and $\alpha = 0^{\circ}$ (Fig. 16(b)), the maximum load attained in both models is significantly different, with the misalignment model achieving only 42% of the maximum load of the reference model. Since the shear stress distribution can be dangerously similar for both cases, significant errors can be introduced in the experimental assessment of G_F^{II}. For instance, if the maximum

load of the model with α = +1.0º (9.5 kN) is used in Eq. (10), the fracture energy in mode-II is calculated as 0.26 N/mm, which is about 17% of the reference value in the pure shear model.

If the wrong fracture energy is now introduced in the pure shear model, i.e. G_F^{II} = 0.26 N/mm, c = 5.0 MPa and k_s = 1500 MPa/mm, the curve corresponding to α_1 = 0 shown in Fig. 16(b) is obtained. It should be highlighted that, if the wrong G_F^{II} value were adopted, a good agreement would still be achieved between numerical and experimental results, concerning both stress distributions and maximum load. Nevertheless, the G_F^{II} value (0.26 N/mm) is quite smaller than the correct one (1.5 N/mm). This similarity of the shear stress distributions, except on a small region near the load edge, points out to a risk of misinterpretation of experimental results.

Detecting the load misalignment in experimental tests can pose difficulties. Only careful monitoring of the CFRP axial strain in the shorter region near the load edge allows for an accurate interpretation of the experimental data. Thus, an incorrect definition of the material parameters is highly probable when the normal component is pointing outwards the substrate. In this case, a G_F^{II} value smaller than the real value would be obtained, leading to the underestimation of the load carrying capacity of the bonded connection.

In the case of t_f = 0.5 mm, the relationship between maximum load with α = +1.0º and α = 0º increases to approximately 52%. Thus, the effect of maximum load decreasing with α > 0º is more important for less thick CFRPs. Results are shown in Fig. 17, for a load level of 65%, leading to 31 kN and 16 kN, respectively for α = −1.0º and α = +1.0º. It is again concluded that the material parameters can be adequately computed in the case of α = −1.0º, whereas significant errors can be introduced in the opposite case. Indeed for α = +1.0º, the maximum load attained is about 52% smaller than the reference one. If Eq. (10) is again used to compute the fracture energy in mode-II, a value of 0.41 N/mm is obtained, which is 27% of the reference value in a pure shear model.

Post-print: Neto, P., Alfaiate, J., Dias-da-Costa, D., Vinagre, J., Mixed-mode fracture and load misalignment on the assessment of FRP-concrete bond connections, *Composite Structures*, Elsevier, 135:49–60, 2016 (doi: 10.1016/j.compstruct.2015.08.139).

In summary, the load misalignment is particularly important when the normal component of the load is pointing outwards and leads to significant changes in the bond behaviour relatively to a pure shear test without misalignment.

5.3. Maximum load and mode-II fracture energy

In this section the variation of the maximum load and the mode-II fracture energy is addressed. For this purpose, new composite thicknesses of 1.4 mm and 6.0 mm are considered in addition to 0.1 mm and 0.5 mm. Furthermore, angle α is now considered to take the following values: 0.5º, 1.0º, 1.5º and 2.0º.

In Fig. 18(a) is shown the loading factor N_{max}/N_u versus CFRP thickness, where N_{max} is the maximum load attained and N_u is the reference maximum load in a pure shear model, obtained without misalignment. From this figure, it is clear that the N_{max}/N_u ratio decreases with increasing misalignment, in some cases attaining a 50% loss in the connection capacity. This effect is even more pronounced for lower thicknesses due to the lever arm, in addition to the peeling stresses.

Eq. (10) can now be used to compute the mode-II fracture energy. In Fig. 18(b) the ratio $G_{F,eq}^{II}/G_F^{II}$ versus CFRP thickness is shown, where $G_{F,eq}^{II}$ and G_F^{II} are, respectively, the mode-II fracture energy with and without misalignment. The conclusions are similar to the loading factor, although a steeper decrease is observed in this case.

In several works, the fracture energy proposed for mode-II can reach 1/3 of the value adopted in this study, see for example [10, 14, 24]. Therefore, the models are now rerun with G_F^{II} = 0.5 N/mm and the corresponding results summarised in Fig. 19. Comparison between Figs. 18 and 19, reveals a similar behaviour, although the load decrease is less steep due to the smaller fracture energy.

Regarding the maximum load value for the connection, a comparison can be established with the following analytical expression proposed by De Lorenzis and Zavarise [10]:

Post-print: Neto, P., Alfaiate, J., Dias-da-Costa, D., Vinagre, J., Mixed-mode fracture and load misalignment on the assessment of FRP-concrete bond connections, *Composite Structures*, Elsevier, 135:49–60, 2016 (doi: 10.1016/j.compstruct.2015.08.139).

$$N_{max} = b_f G_F \frac{\sqrt{\left(\frac{E_f t_f}{G_F}\right)^2 (1-\cos\alpha)^2 + 2\frac{E_f t_f}{G_F}\left(\sin^2\alpha + \frac{\cos^2\alpha}{\frac{G_F^{II}}{G_F}}\right)} - \frac{E_f t_f}{G_F}(1-\cos\alpha)}{\sin^2\alpha + \frac{\cos^2\alpha}{\frac{G_F^{II}}{G_F}}}, \quad (14)$$

which leads to the results shown in Figs. 20(a) and (b), respectively for G_F^{II} = 1.5 N/mm and G_F^{II} = 0.5 N/mm. In this case, although both numerical and analytical models behave similarly, the load ratio seems to decrease faster in the latter approach.

5.4. Effective bond length

The accurate definition of bond length varies among different authors. For instance, Nakaba, Kanakubo [41] define the effective bond length as the distance between two points of the shear stress diagram which corresponds to 10% of the cohesion. On the other hand, Brosens [46] and Yuan, Wu [20] define this length such that it corresponds to 97% of the maximum load, whereas this ratio increases to 99% in [51]. In this Section, the effective bond length is defined as the distance between two points of the shear stress diagram corresponding to 1% of the cohesion, obtained for 97% of the maximum load.

In Fig. 21 the variation of the effective bond length ratio $l_{beff,\alpha}/l_{beff}$ with respect to the CFRP thickness is shown, where $l_{beff,\alpha}$ is the effective bond length in the model with load misalignment and l_{beff} is the effective bond length for α = 0. This ratio decreases for higher values of α and smaller thicknesses.

6. Conclusions

The simulation of CFRP to concrete bond connection requires the definition of several material properties, namely: *i*) shear and peeling stiffness; *ii*) cohesion; *iii*) tensile strength; and *iv*) fracture energies, both under mode-I and mode-II fracture. In the literature, significant variations for the definition of these parameters can be found. The contribution to these variations of mixed-mode

Post-print: Neto, P., Alfaiate, J., Dias-da-Costa, D., Vinagre, J., Mixed-mode fracture and load misalignment on the assessment of FRP-concrete bond connections, *Composite Structures*, Elsevier, 135:49–60, 2016 (doi: 10.1016/j.compstruct.2015.08.139).

fracture behaviour due to: *i*) the CFRP thickness and *ii*) load misalignment, was herein analysed. The main objective was to quantify the relevance of the load misalignment in pure shear test models and corresponding errors in the interpretation of existing experimental data. It was also intended to evaluate the importance of the mixed-mode and mode-II fracture energies in the analysis of existing experimental data, including the identification of the role of all parameters in the maximum load and effective bond length attained by the connection.

The relevance of the load misalignment in the interpretation of experimental tests was assessed by means of a parametric study. In all cases, the misalignment angle was limited to 2º, since this value corresponds to an error that can be easily introduced in experimental set-ups. If, as a result of the misalignment angle, the load points inwards the substrate, the maximum load and stress distribution is only modified within a short neighbourhood from the applied load. However, in the case of a positive misalignment, important differences were found in the connection strength. In this situation, the load carrying capacity decreases significantly and in some cases it can reach half of the reference strength. A similar trend was identified for the effective bond length due to a more premature failure. This decrease in load carrying capacity can lead to important deviations in the evaluation of mode-II fracture energy. This can be the reason why this latter parameter exhibits an important dispersion in the literature. Therefore, all available experimental data has to be carefully interpreted.

The quantification of cohesion from experimental tests was also achieved. In this case, if compressive stresses are introduced by the load misalignment, shear stresses higher than the cohesion are obtained along a small length.

The shear stiffness appears to be the parameter with the widest range of values when compared to cohesion and mode-II fracture energy. This parameter depends mainly on the adhesive [36, 45] and, for larger values, its impact on the maximum load and tangential stresses could be neglected.

In the assessment of the bond behaviour due to a load misalignment, the influence of the CFRP thickness was also taken into account. This allows for the consideration of the adherent bending

Post-print: Neto, P., Alfaiate, J., Dias-da-Costa, D., Vinagre, J., Mixed-mode fracture and load misalignment on the assessment of FRP-concrete bond connections, *Composite Structures*, Elsevier, 135:49–60, 2016 (doi: 10.1016/j.compstruct.2015.08.139).

stiffness in the numerical analysis, as well as the lever arm developed in the composite thickness. This lever arm by itself leads to normal compressive stresses in the interface, which increase with the thickness of the CFRP. These compressive stresses have a favourable contribution to the load carrying capacity of the glued connection. Therefore it is possible to conclude that the bond strength reduction mentioned above is smaller for higher thicknesses, due to:

i) compressive stress, as a result of the lever arm developed along the CFRP thickness;

ii) composite bending stiffness leading to a larger length where the peeling stresses are distributed, consequently decreasing the tensile stress level supported by the interface.

Finally, it should be mentioned that due to the bending stiffness this effect tends to be less important for increasing thicknesses of the strengthening material, for instance when switching from CFRP sheets to CFRP laminates.

Acknowledgements

Financial support has been provided by the Portuguese Fundação para a Ciência e a Tecnologia (FCT) of the Portuguese Ministry of Science and Technology and Higher Education (PROTEC 2009). Support was also provided by FEDER funds through the Operational Programme for Competitiveness Factors – COMPETE – and by Portuguese funds through FCT – Portuguese Foundation for Science and Technology under Project No. FCOMP-01-0124-FEDER-020275 (FCT ref. PTDC/ECM/119214/2010). D. Dias-da-Costa would like to acknowledge the support from the Australian Research Council through its Discovery Early Career Researcher Award (DE150101703) and from the Faculty of Engineering & Information Technologies, The University of Sydney, under the Faculty Research Cluster Program.

Post-print: Neto, P., Alfaiate, J., Dias-da-Costa, D., Vinagre, J., Mixed-mode fracture and load misalignment on the assessment of FRP-concrete bond connections, *Composite Structures*, Elsevier, 135:49–60, 2016 (doi: 10.1016/j.compstruct.2015.08.139).

References

[1] Xue WC, Zeng L, Tan Y. Experimental studies on bond behaviour of high strength CFRP plates. Composites Part B-Engineering. 2008;39:592-603.
[2] Mazzotti C, Savoia M, Ferracuti B. An experimental study on delamination of FRP plates bonded to concrete. Construction and Building Materials. 2008;22:1409-21.
[3] Malek AM, Saadatmanesh H, Ehsani MR. Prediction of failure load of R/C beams strengthened with FRP plate due to stress concentration at the plate end. Aci Structural Journal. 1998;95:142-52.
[4] Täljsten B. Plate bonding: strengthening of existing concrete structures with epoxy bonded plates of steel or fibre reinforced plastics [Doctoral Thesis]: Luleå University of Technology, 1994.
[5] Chajes MJ, Finch WW, Januszka TF, Thomson TA. Bond and force transfer of composite material plates bonded to concrete. Aci Structural Journal. 1996;93:208-17.
[6] Bizindavyi L, Neale KW. Transfer Lengths and Bond Strengths for Composites Bonded to Concrete. Journal of Composites for Construction. 1999;3:7.
[7] Achintha M, Burgoyne CJ. Fracture mechanics of plate debonding: Validation against experiment. Construction and Building Materials. 2011;25:2961-71.
[8] Rabinovitch O, Frostig Y. Closed-form High-order Analysis of RC Beams Strengthened with FRP Strips. Journal of Composites for Construction-ASCE. 2000;4:9.
[9] Wu Z, Niu H. Shear transfer along FRP-concrete interface in flexural members. Journal of Material, Concrete Structures and Pavements, JSCE. 2000;49:14.
[10] De Lorenzis L, Zavarise G. Modeling of mixed-mode debonding in the peel test applied to superficial reinforcements. International Journal of Solids and Structures. 2008;45:5419-36.
[11] Bazant ZP, Pfeiffer PA. Shear Fracture tests of concrete. Materials and Structures. 1986;19:111-21.
[12] Ozbolt J, Reinhardt HW, Xu S. Numerical studies of the double-edge notched mode-II geometry. In: Mihashi H, Rokugo K, editors. FRAMCOS-3. Japan1998. p. 773-82.
[13] Coronado CA, Lopez MM. Numerical Modeling of Concrete-FRP Debonding Using a Crack Band Approach. Journal of Composites for Construction. 2010;14:11-21.
[14] Savoia M, Ferracuti B, Vincenzi L. Inverse Analysis for the Calibration of FRP-Concrete Interface Law. Advances in Structural Engineering. 2009;12:613-25.
[15] Wu YF, Zhou ZQ, Yang QD, Chen WQ. On shear bond strength of FRP-concrete structures. Engineering Structures. 2010;32:897-905.
[16] Pellegrino C, Modena C. Influence of FRP Axial Rigidity on FRP-Concrete Bond Behaviour: An Analytical Study. Advances in Structural Engineering. 2009;12:639-49.
[17] Wang JL. Cohesive-bridging zone model of FRP-concrete interface debonding. Engineering Fracture Mechanics. 2007;74:2643-58.
[18] Horiguchi T, Saeki N. Effect of test methods and quality of concrete on bond strength of CFRP sheet. Third International Symposium on Non-Metallic (FRP) Reinforcement for Concrete Structures (FRPRCS-3). Japan Concrete Institute, Sapporo, Japan1997. p. 265-70.
[19] De Lorenzis L, Zavarise G. Debonding analysis of thin plates from curved substrates. Engineering Fracture Mechanics. 2010;77:3310-28.
[20] Yuan H, Wu ZS, Yoshizawa H. Theoretical Solutions on Interfacial Stress Transfer of Externally Bonded Steel/Composite Laminates. Journal of Structural Mechanics and Earthquake Engineering - JSCE. 2001:27-39.
[21] Ferracuti B, Savoia M, Mazzotti C. Interface law for FRP-concrete delamination. Composite Structures. 2007;80:523-31.
[22] Chen JF, Teng JG. Anchorage strength models for FRP and steel plates bonded to concrete. Journal of Structural Engineering-Asce. 2001;127:784-91.
[23] Ebead UA, Neale KW. Mechanics of fibre-reinforced polymer-concrete interfaces. Canadian Journal of Civil Engineering. 2007;34:367-77.

Post-print: Neto, P., Alfaiate, J., Dias-da-Costa, D., Vinagre, J., Mixed-mode fracture and load misalignment on the assessment of FRP-concrete bond connections, *Composite Structures*, Elsevier, 135:49–60, 2016 (doi: 10.1016/j.compstruct.2015.08.139).

[24] Ali-Ahmad MK, Subramaniam KV, Ghosn M. Analysis of Scaling and Instability in FRP-Concrete Shear Debonding for Beam-Strengthening Applications. Journal of Engineering Mechanics. 2007;133:58-65.
[25] Carloni C, Subramaniam KV. Direct determination of cohesive stress transfer during debonding of FRP from concrete. Composite Structures. 2010;93:184-92.
[26] Wu ZS, Yuan H, Niu HD. Stress transfer and fracture propagation in different kinds of adhesive joints. Journal of Engineering Mechanics-Asce. 2002;128:562-73.
[27] Tounsi A, Daouadji TH, Benyoucef S, Bedia EAA. Interfacial stresses in FRP-plated RC beams: Effect of adherend shear deformations. International Journal of Adhesion and Adhesives. 2009;29:343-51.
[28] Choi HT, West JS, Soudki KA. Analysis of the flexural behavior of partially bonded FRP strengthened concrete beams. Journal of Composites for Construction. 2008;12:375-86.
[29] Wang YC, Chen CH. Analytical study on reinforced concrete beams strengthened for flexure and shear with composite plates. Composite Structures. 2003;59:137-48.
[30] Pisani MA. Evaluation of bending strength with FRP of RC beams strengthened with FRP sheets. Journal of Composites for Construction. 2006;10:313-20.
[31] Lu XZ, Jiang JJ, Teng JG, Ye LP. Finite element simulation of debonding in FRP-to-concrete bonded joints. Construction and Building Materials. 2006;20:412-24.
[32] Volkersen O. Die Nietkraftverteilung in zugbeanspruchten nietverbindungen mit konstanten laschenquerschnitten. Luftfahrtforschung. 1938;15:41-7.
[33] Bresson J. Nouvelles recherches et applications concernant l'utilisation des collages dans les structures. Béton plaqué, Annales de l'Institut Technique du Batiment et des Travaux Publics. 1971;278:22-55.
[34] Kaiser H. Bewehren von stahlbeton mit kohlenstoffaserverstärkten epoxidharzen. Zurich, Switzerland: Eidgenössische Technische Hochschule Zürich, 1989.
[35] Ladner M, Weder C. Concrete Structures with Bonded External Reinforcement. Dübendorf, Switzerland: Swiss Federal Laboratories for Materials Testing and Research, EMPA; 1981. p. 60.
[36] Lee YJ, Boothby TE, Bakis CE, Nanni A. Slip modulus of FRP sheets bonded to concrete. ASCE Journal of Composites for Construction. 1999;3:161-7.
[37] Holzenkämpfer P. Ingenieurmodelle des verbunds geklebter bewehrung für betonbauteile [Doctoral thesis]. Germany: IBMB, TU Braunschweig, 1994.
[38] Neubauer U, Rostásy F. Design aspects of concrete structures strengthened with externally bonded CFRP plates. 7th International Conference on Structural Faults and Repairs. Edinburgh, Scotland: ECS Publications; 1997. p. 109-18.
[39] Coronado CA, Lopez MM. Damage approach for the prediction of debonding failure on concrete elements strengthened with FRP. Journal of Composites for Construction. 2007;11:391-400.
[40] Neto P, Alfaiate J, Almeida JR, Pires EB. The influence of mode II fracture on concrete strengthened with CFRP. Computers & Structures. 2004;82:1495-502.
[41] Nakaba K, Kanakubo T, Furuta T, Yoshizawa H. Bond behavior between fiber-reinforced polymer laminates and concrete. Aci Structural Journal. 2001;98:359-67.
[42] Popovics S. A numerical approach to the complete stress-strain curve of concrete. Cement and Concrete Research. 1973;3:583-99.
[43] Petersson P-E. Crack growth and development of fracture zones in plain concrete and similar materials [Doctoral Thesis]. Div of Building Materials LTH, Lund university: Lund university, 1981.
[44] Neto P, Alfaiate J, Vinagre J. Numerical modelling of concrete beams reinforced with pre-stressed CFRP. International Journal of Fracture. 2009;157:159-73.
[45] De Lorenzis L, Miller B, Nanni A. Bond of fiber-reinforced polymer laminates to concrete. ACI Materials Journal. 2001;98:256-64.
[46] Brosens K. Anchorage of externally bonded steel plates and CFRP laminates for the strengthening of concrete elements [Doctoral Thesis]: K. U. Leuven, 2001.

Post-print: Neto, P., Alfaiate, J., Dias-da-Costa, D., Vinagre, J., Mixed-mode fracture and load misalignment on the assessment of FRP-concrete bond connections, *Composite Structures*, Elsevier, 135:49–60, 2016 (doi: 10.1016/j.compstruct.2015.08.139).

[47] Ali-Ahmad M, Subramaniam K, Ghosn M. Experimental Investigation and Fracture Analysis of Debonding between Concrete and FRP Sheets. Journal of Engineering Mechanics-ASCE. 2006;132:914-23.
[48] Arduini M, Nanni A. Behavior of Precracked RC Beams Strengthened with Carbon FRP Sheets. Journal of Composites for Construction - ASCE. 1997;1:63-70.
[49] Arduini M, DiTommaso A, Nanni A. Brittle failure in FRP plate and sheet bonded beams. Aci Structural Journal. 1997;94:363-70.
[50] Pellegrino C, Modena C. An experimentally based analytical model for the shear capacity of FRP-strengthened reinforced concrete beams. Mechanics of Composite Materials. 2008;44:231-44.
[51] Lu XZ, Teng JG, Ye LP, Jiang JJ. Bond-slip models for FRP sheets/plates bonded to concrete. Engineering Structures. 2005;27:920-37.
[52] Travassos NC. Caracterização do comportamento da Ligação CFRP-betão [Master Thesis]: Instituto Superior Técnico, Technical University of Lisbon, 2002.
[53] Lourenço PB, Rots JG. Multi-surface interface model for the analysis of masonry structures. Journal of Engineering Mechanics - ASCE. 1997;123:660-8.
[54] Alfaiate J, Almeida JR. Crack Evolution in Confined Masonry Walls In: Idelshon SR, Oñate E, Dvorkin E, editors. Computational Mechanics: New Trends and Applications, CIMNE. Barcelona, Spain1998. p. .
[55] Dias-da-Costa D, Alfaiate J, Júlio ENBS. FE modeling of the interfacial behaviour of composite concrete members. Construction and Building Materials. 2012;26:233-43.
[56] Neto P, Alfaiate J, Vinagre J. Modeling the behavior of reinforced concrete beams strengthened with FRP. In: Motasoares CA, Martins JAC, Rodrigues HC, Ambrósio JAC, Pina CAB, Motasoares CM, et al., editors. III European Conference on Computational Mechanics Solids, Structures and Coupled Problems in Engineering, ECCM2006. National Laboratory for Civil Engineering, Lisboa, Portugal: Springer Netherlands; 2006.
[57] Alfaiate J, Pires EB. Mode-I and mixed-mode non-prescribed discrete crack propagation in concrete. In: Mihashi H, Rokugo K, editors. FRAMCOS-3. Japan1998. p. 739-48.
[58] Gálvez JC, Cendón DA, Planas J, Guinea GV, Elices M. Fracture of concrete under mixed loading - experimental results and numerical prediction. In: Mihashi H, Rokugo K, editors. FRAMCOS-3. Japan1998. p. 729-38.

Post-print: Neto, P., Alfaiate, J., Dias-da-Costa, D., Vinagre, J., Mixed-mode fracture and load misalignment on the assessment of FRP-concrete bond connections, *Composite Structures*, Elsevier, 135:49–60, 2016 (doi: 10.1016/j.compstruct.2015.08.139).

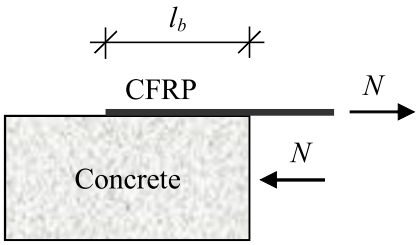

Fig. 1: Single Shear Test under tension-compression.

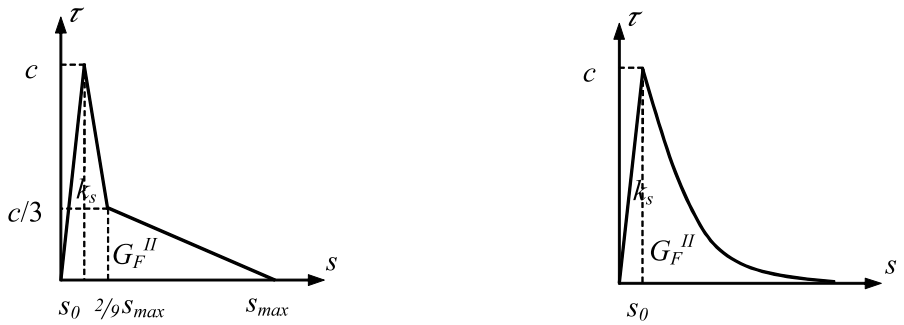

a) b)

Fig. 2: Interface bond-slip laws adopted in previous works [40, 56] with: (a) a bilinear; and (b) an exponential softening branch.

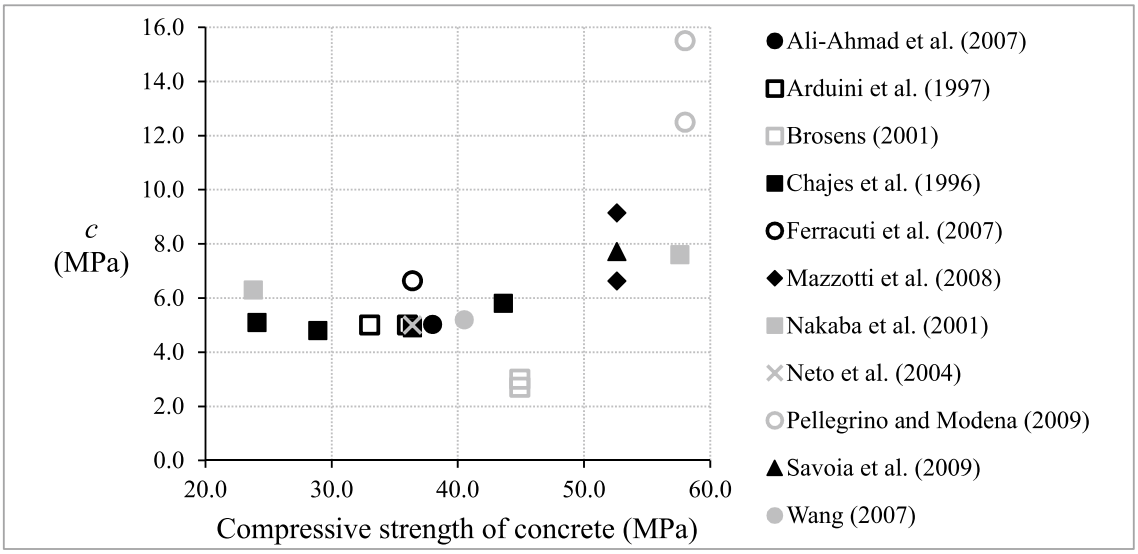

Fig. 3: Cohesion vs. concrete compressive strength.

Post-print: Neto, P., Alfaiate, J., Dias-da-Costa, D., Vinagre, J., Mixed-mode fracture and load misalignment on the assessment of FRP-concrete bond connections, *Composite Structures*, Elsevier, 135:49–60, 2016 (doi: 10.1016/j.compstruct.2015.08.139).

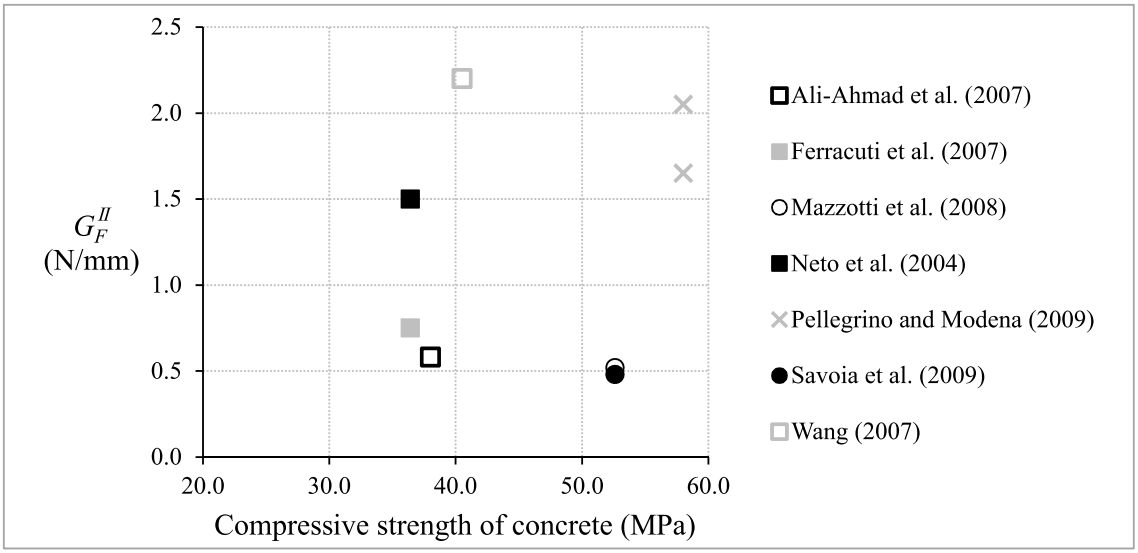

Fig. 4: Fracture energy in mode-II vs. concrete compressive strength.

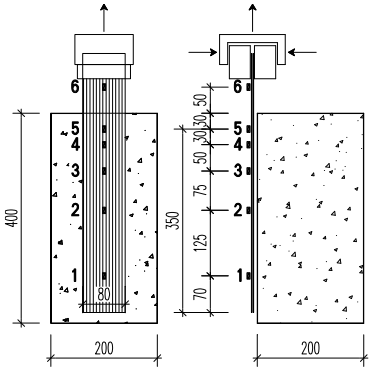

Fig. 5: Shear model on concrete joint externally strengthened with CFRP [52].

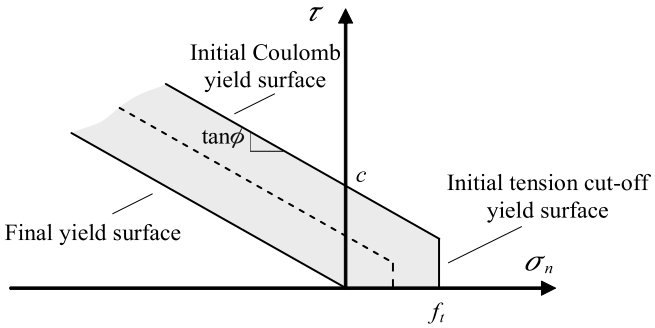

Fig. 6: Yield surfaces adopted for the interface.

Post-print: Neto, P., Alfaiate, J., Dias-da-Costa, D., Vinagre, J., Mixed-mode fracture and load misalignment on the assessment of FRP-concrete bond connections, *Composite Structures*, Elsevier, 135:49–60, 2016 (doi: 10.1016/j.compstruct.2015.08.139).

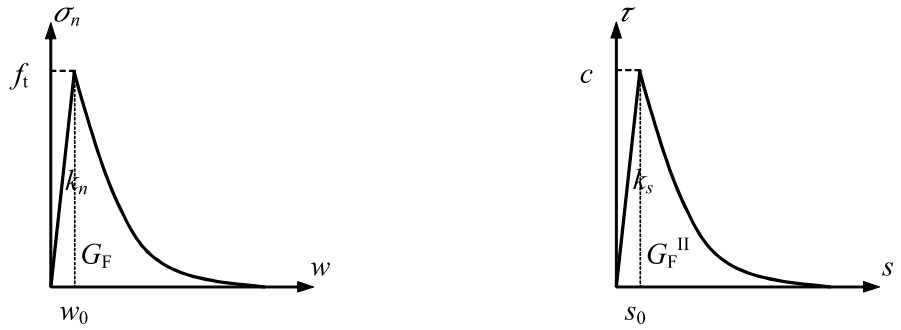

a) b)

Fig. 7: Constitutive relations for the interface: (a) normal; and (b) tangential components

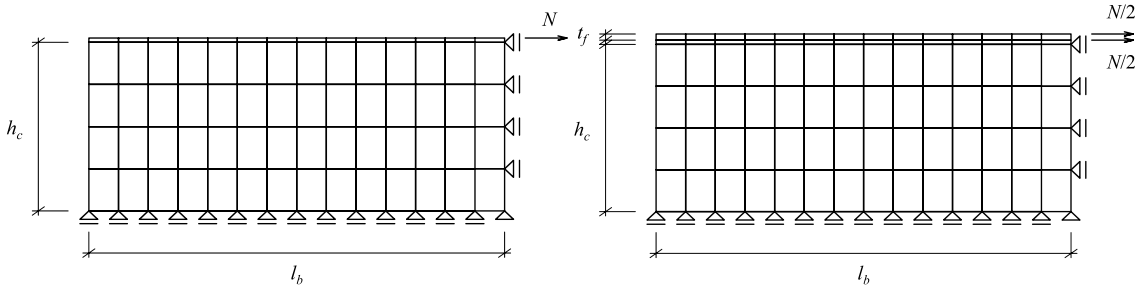

a) b)

Fig. 8: Schematic representation of the meshes adopted in the fracture models for: (a) pure mode-II; and (b) mixed mode.

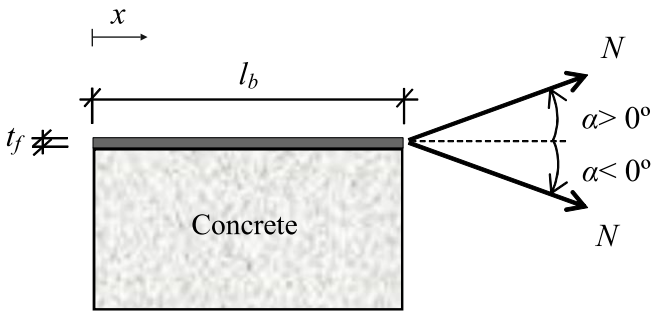

Fig. 9: Definition of the load slope angle, α.

Post-print: Neto, P., Alfaiate, J., Dias-da-Costa, D., Vinagre, J., Mixed-mode fracture and load misalignment on the assessment of FRP-concrete bond connections, *Composite Structures*, Elsevier, 135:49–60, 2016 (doi: 10.1016/j.compstruct.2015.08.139).

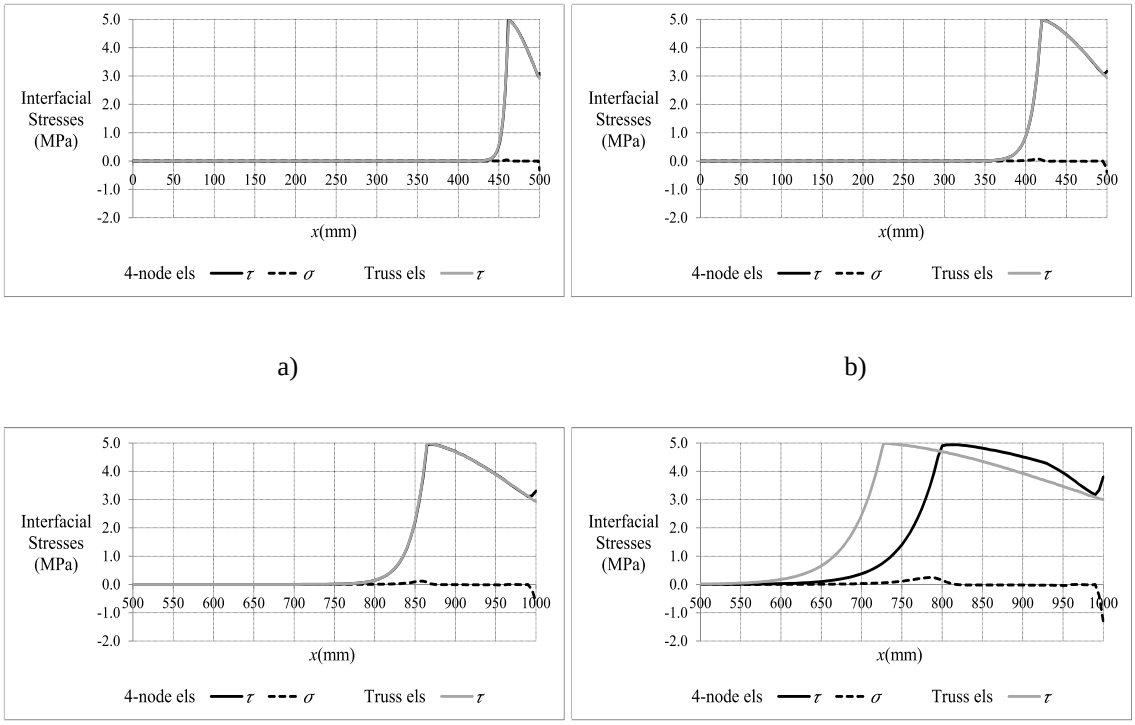

Fig. 10: Interfacial stresses for 65% of the maximum load: (a) t_f = 0.1 mm (N = 15 kN); (b) t_f = 0.5 mm (N = 31 kN); (c) t_f = 1.4 mm (N = 52 kN); and (d) t_f = 6.0 mm (N = 106 kN).

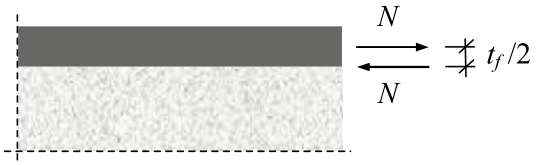

Fig. 11: Lever arm developing in the CFRP thickness.

Post-print: Neto, P., Alfaiate, J., Dias-da-Costa, D., Vinagre, J., Mixed-mode fracture and load misalignment on the assessment of FRP-concrete bond connections, *Composite Structures*, Elsevier, 135:49–60, 2016 (doi: 10.1016/j.compstruct.2015.08.139).

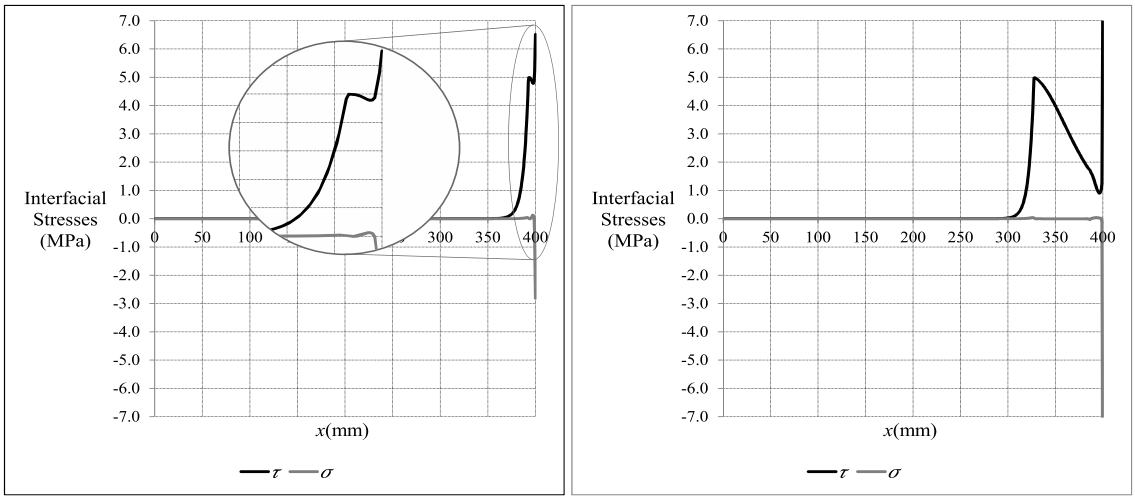

a) b)

Fig.12: Interfacial stresses with t_f = 0.1 mm and α = −1.0º for: (a) 20% of the maximum load (F = 5 kN); and (b) 90% of the maximum load (F = 20 kN).

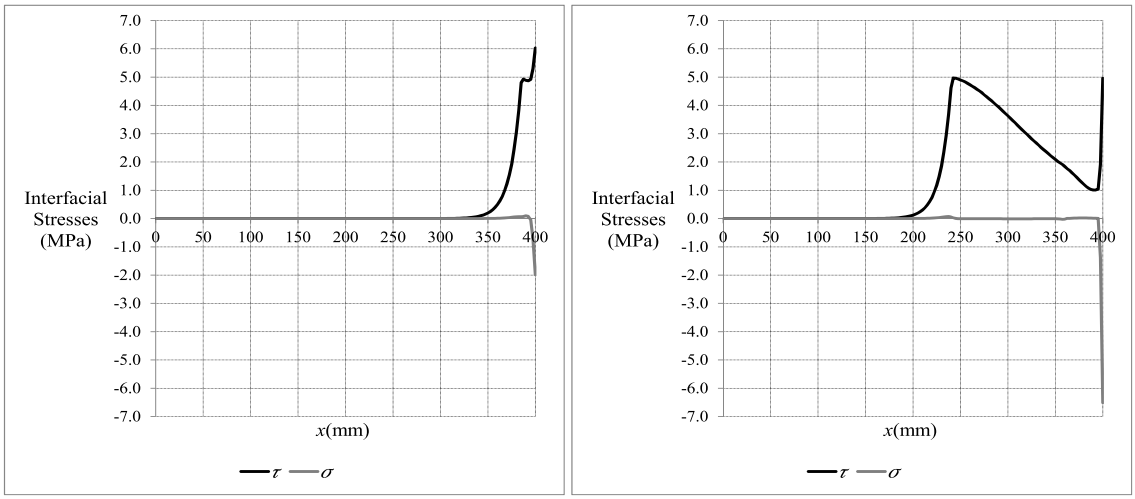

a) b)

Fig. 13: Interfacial stresses with t_f = 0.5 mm and α = −1.0º for: (a) 20% of the maximum load (N = 10 kN); and (b) 90% of the maximum load (N = 43 kN).

Post-print: Neto, P., Alfaiate, J., Dias-da-Costa, D., Vinagre, J., Mixed-mode fracture and load misalignment on the assessment of FRP-concrete bond connections, *Composite Structures*, Elsevier, 135:49–60, 2016 (doi: 10.1016/j.compstruct.2015.08.139).

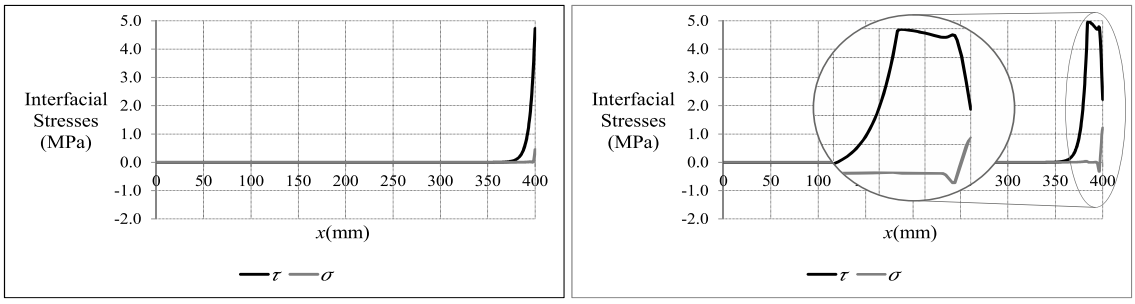

a) b)

Fig. 14: Interfacial stresses with t_f = 0.1 mm and α = 1.0º for: (a) 20% of the maximum load (N = 2 kN); and (b) 90% of the maximum load (N = 8.5 kN).

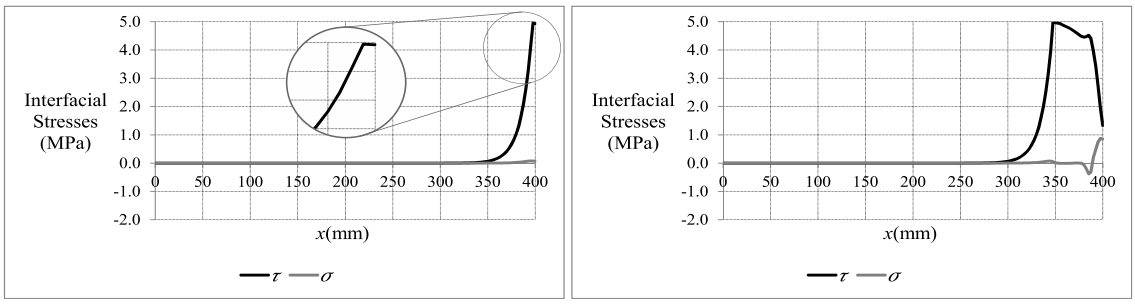

a) b)

Fig. 15: Interfacial stresses with t_f = 0.5 mm and α = 1.0º for: (a) 20% of the maximum load (N = 5 kN); and (b) 90% of the maximum load (N = 22.5 kN).

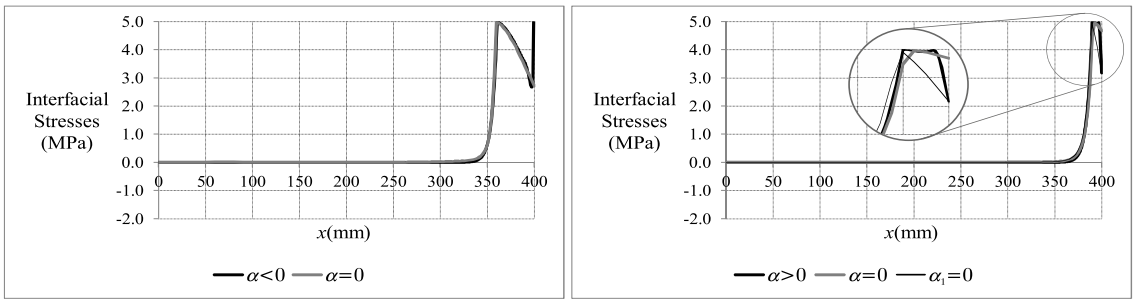

a) b)

Fig. 16: Shear stresses with t_f = 0.1 mm for 65% of the maximum load obtained with: (a) α = -1.0º and (b) α = 1.0º.

Post-print: Neto, P., Alfaiate, J., Dias-da-Costa, D., Vinagre, J., Mixed-mode fracture and load misalignment on the assessment of FRP-concrete bond connections, *Composite Structures*, Elsevier, 135:49–60, 2016 (doi: 10.1016/j.compstruct.2015.08.139).

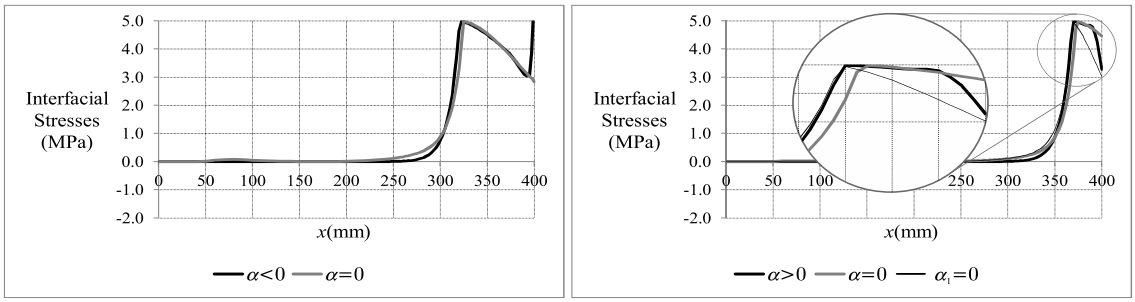

a) b)

Fig. 17: Shear stresses with t_f = 0.5 mm for 65% of the maximum load: (a) α = -1.0º; and (b) α = 1.0º.

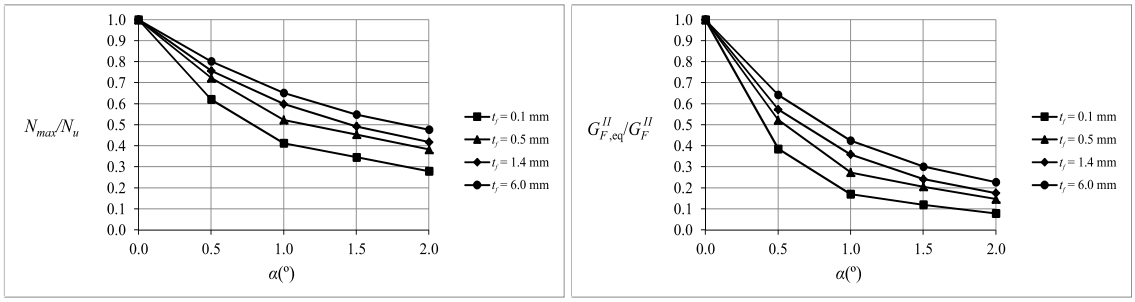

a) b)

Fig. 18: Effect of the load misalignment with G_F^{II} = 1.5 N/mm on the: (a) maximum load; and (b) fracture energy, for different thicknesses.

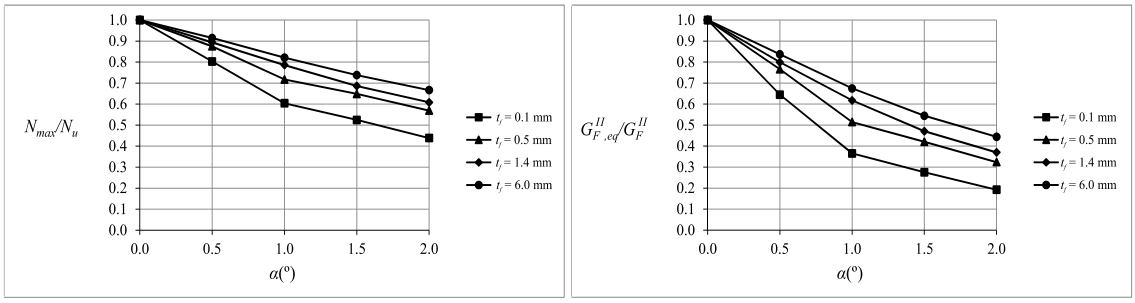

a) b)

Fig. 19: Effect of the load misalignment with G_F^{II} = 0.5 N/mm on the: (a) maximum load; and (b) fracture energy, for different thicknesses.

Post-print: Neto, P., Alfaiate, J., Dias-da-Costa, D., Vinagre, J., Mixed-mode fracture and load misalignment on the assessment of FRP-concrete bond connections, *Composite Structures*, Elsevier, 135:49–60, 2016 (doi: 10.1016/j.compstruct.2015.08.139).

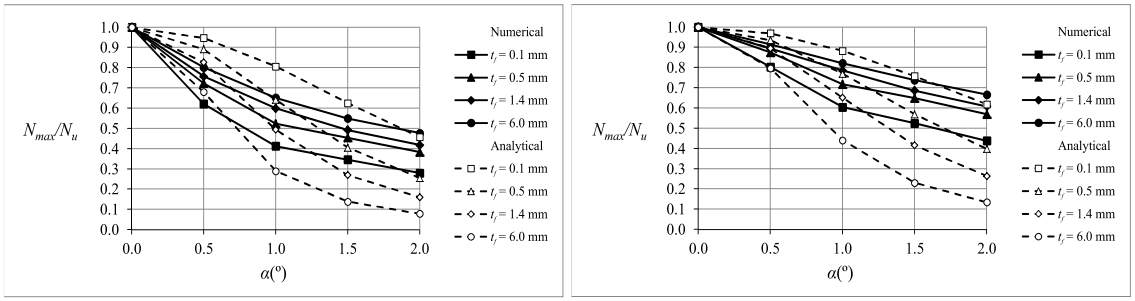

a) b)

Fig. 20: Effect of the load misalignment on the maximum load, for different thicknesses, with: (a) G_F^{II} = 1.5 N/mm; and (b) G_F^{II} = 0.5 N/mm.

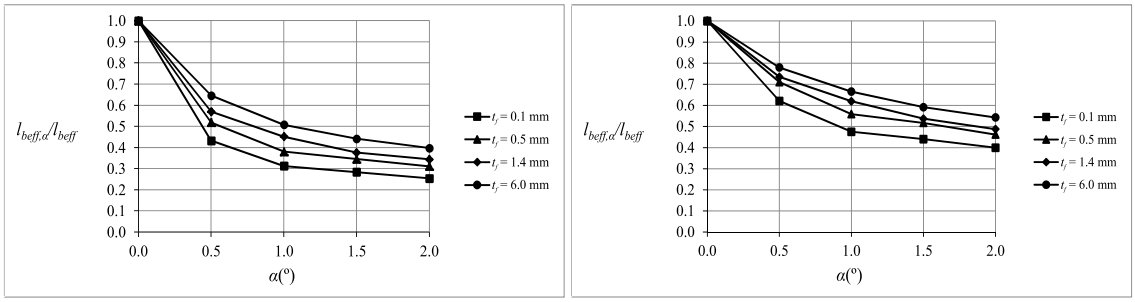

a) b)

Fig. 21: Effect of the load misalignment on the effective bond length, for different thicknesses, with: (a) G_F^{II} = 1.5 N/mm and (b) G_F^{II} = 0.5 N/mm.

Post-print: Neto, P., Alfaiate, J., Dias-da-Costa, D., Vinagre, J., Mixed-mode fracture and load misalignment on the assessment of FRP-concrete bond connections, *Composite Structures*, Elsevier, 135:49–60, 2016 (doi: 10.1016/j.compstruct.2015.08.139).